Analysis of Factors Affecting Strain Distribution in Geosynthetics

M. Emin Kutay[1]; Murat Guler[2]; and Ahmet H. Aydilek[3]

Abstract: Localized strains due to production defects, seams, and punctured zones significantly affect mechanical performance of geosynthetic materials. Accurate determination of localized strains becomes particularly important for quality control/quality assurance evaluation of these materials and may play a critical role in design problems. A battery of tensile tests was conducted on 12 different geosynthetics to assess the effects of seam type, puncture, and clamping techniques on strain distributions. Digital images of the geosynthetic specimens were captured during testing, and the analyses of time-lapsed images were performed using two optical flow techniques to define strain distributions within specimens as well as in the vicinity of grip locations and seam zones. The results indicated that the optical flow techniques used in this study can successfully define the distribution of strains in a geosynthetic test specimen during tensile testing. The magnitude of lateral strains was small in polypropylene wovens and geogrids, whereas it was significant in polyester wovens and nonwovens. Large strains developed in the vicinity of seams regardless of the clamping technique used. The strains at the seam zones measured with hydraulic grips were significantly higher than those measured with roller grips. Sewn geosynthetics generally experienced lower lateral strain-to-axial strain ratios. The average axial strain appears to be insensitive to puncture regardless of the type of geosynthetics considered or the clamping technique used.

DOI: 10.1061/(ASCE)1090-0241(2006)132:1(1)

CE Database subject headings: Strain distribution; Imaging techniques; Geosynthetics; Geomaterials.

Introduction

In the design process, geosynthetic materials are expected to offer certain mechanical properties that will provide satisfactory performance when exposed to field conditions. Among various mechanical performance tests available today, the wide-width tensile test (*ASTM D 4595*) (ASTM 2001b) is the most commonly used test in design applications (Koerner 1999). The strength properties determined from this test are defined at a particular strain or elongation level and strains are usually calculated on an average basis using only uniaxial deformations. The cross-head displacement method, which measures the separation distance between two tension grips during testing, is the current state of practice for determining the overall strain. This method, however, does not provide any information about localized in-plane strains that developed during tension (Bais-Singh and Goswami 1996). Also, the method does not provide lateral strains developed due to Poisson's effect that is typically encountered in nonwoven geotextiles. On the other hand, an accurate determination of such in-plane strains becomes particularly critical for design applications in which the long-term durability of geosynthetics is of primary concern. The localized in-plane strains that affect the overall mechanical performance of geosynthetics may occur due to the presence of seams, punctured zones, or possible defects generated during production.

Existing research has indicated that the strains in geotextiles can reach significant levels during their service life when the geotextile is used as a separator or a reinforcement agent. Billard and Wu (1991) measured excess localized strains in full scale model testing of geotextile-reinforced retaining walls. Their results indicated that the strains in geotextile located in the upper part of the wall were not constant and varied from 2 to 17%. In another study, Raymond (1994) investigated the localized strains for geotextiles used as a separator between railroad stone ballast and soft underground layer. In such applications, large localized strains can be developed by the puncture and bursting effects of stone ballast due to dynamic wheel loads and the strains during the rupture of nonwoven geotextiles may reach significant levels.

The lateral strains (contractions) developed under tensile loads are of interest especially in soil reinforcement applications since the amount of contraction is likely to be restrained by the soil in the field (Shinoda and Bathurst 2004a). Therefore, it is important to determine the axial strain levels at which the amount of contraction becomes significant. The determination of lateral strains becomes more important for some of the critical applications in which the geosynthetic acts as a reinforcement agent, such as in capping of contaminated high water content geomaterials. The distribution of strains can be critical in these applications, since the geotextile is stretched significantly even under low equipment loads mainly due to the presence of a foundation with extremely

[1]Graduate Research Assistant, Dept. of Civil and Environmental Engineering, Univ. of Maryland, 1173 Glenn Martin Hall, College Park, MD 20742. E-mail: kutay@wam.umd.edu

[2]Assistant Professor, Dept. of Civil Engineering, Middle East Technical Univ., Ankara, Turkey. E-mail: gmurat@metu.edu.tr

[3]Assistant Professor, Dept. of Civil and Environmental Engineering, 1163 Glenn Martin Hall, Univ. of Maryland, College Park, MD 20742 (corresponding author). E-mail: aydilek@eng.umd.edu

Note. Discussion open until June 1, 2006. Separate discussions must be submitted for individual papers. To extend the closing date by one month, a written request must be filed with the ASCE Managing Editor. The manuscript for this paper was submitted for review and possible publication on November 2, 2004; approved on July 18, 2005. This paper is part of the ***Journal of Geotechnical and Geoenvironmental Engineering***, Vol. 132, No. 1, January 1, 2006. ©ASCE, ISSN 1090-0241/2006/1-1–11/$25.00.

low bearing pressures and development of mud waves. Such unexpected variations in strains may affect the overall stability of the structure, leading to localized or global stability problems. Furthermore, significant variation in strains may cause intolerable amounts of differential settlement in the cap overlying the high water content geomaterial (Edil and Aydilek 2001). Large differences in in-plane strain components and their effects to the stability of structures may necessitate an adjustment of the allowable geosynthetic strength by the cumulative strength reduction factor to a level that closely represents the field working conditions of the geosynthetics.

Localized strains have been occasionally determined in the laboratory using strain gages and extensometers. One disadvantage of using these devices is the disruption of filaments or yarns in geosynthetics because they often cause additional strains on test specimens. Furthermore, the measurable strain levels by these gages are usually far less than the strains attained in typical geosynthetic tension tests (Chew et al. 2000). As an alternative, laser beam and infrared sensors have been used in recent years to evaluate the strain distributions in geosynthetics by means of noncontact measurement methods (Skochdopole et al. 2000). However, similar to the methods that provide contact measurements, these sensors define only average axial strains along a selected gage length. Due to the aforementioned limitations in the current methodologies, the localized strain zones usually remain undetected in the wide-width tensile testing and, consequently, the incomplete characterization of mechanical performance may eventually lead to either unconservative design or possible failures of geosynthetics during service conditions.

Previous studies clearly indicated that an evaluation of strain distributions without causing disturbance in geosynthetics is needed and image-based techniques can be successfully adapted for this purpose (Aydilek et al. 2004; Shinoda and Bathurst 2004b). To respond to this need, a laboratory study that includes wide-width tensile tests was conducted to investigate the effects of seam type, puncture, and specimen clamping methods on the strain response of different geosynthetics. The digital images of geosynthetics captured during tension tests were analyzed using two image-based optical flow methods to define the strain fields: a commonly used technique normalized cross correlation (NCC) and a newly developed technique block-based minimum absolute difference (BMAD) (Aydilek et al. 2004), and the results are presented in the following sections.

Materials and Methods

Specimen Preparation and Image Acquisition

One nonwoven geotextile, seven woven geotextiles, and four geogrids were employed in the testing program. The two monofilament polypropylene (PP) wovens with relatively lower ultimate strengths (39–47 kN/m), W1 and W2, are generally used in reinforcement and filtration applications in which low stresses are exerted by the overlying structure, e.g., capping of contaminated sludges. The remaining five wovens are manufactured from either PP or polyester (PET) and had multifilament or fibrillated yarn filaments in their structure. These geotextiles are generally used in reinforcement applications requiring medium to high strengths. Geogrids used in this study had a knitted multifilament structure and were manufactured from polyester (PET). Sewn specimens of selected geotextiles were also employed in the testing program. Those geotextiles were sewn using butterfly, flat, and J-type seams with type 401 two-thread chain-stitching technique. All of the geosynthetics were subjected to wide-width tensile tests using two different types of clamping: hydraulic and roller grips. Duplicate specimens were tested from each type for quality control purposes. The properties of the geosynthetics and a summary of the testing program are given in Table 1.

A MTS Sintech loading frame equipped with a 66 kN and a 286 kN capacity load cell was used for testing with hydraulic and roller grips, respectively. The selected strain rate was 11%/min for specimens tested in the hydraulic grips. A strain rate of 10%/min and 12%/min were utilized for sewn and unsewn specimens, respectively, when roller grips were used for clamping. The dimensions of both sewn and unsewn specimens tested with the hydraulic grips were selected as 457 mm by 200 mm. The specimens prepared for roller grips were trimmed to

Table 1. Properties of Geosynthetics Tested

				Wide width tensile strength (kN/m)						
Type	Geosynthetic ID[a]	Structure[b]	Mass per unit area (g/m^2)	At 5% strain	Ultimate strength	Unsewn[c]	Flat seam[c]	J seam[c]	Butterfly seam[c]	Punctured[c]
Nonwoven Geotextile	NW	NP, PP	278	NA[c]	NA[c]	R,H	H	H	H	R,H
Woven geotextiles	W1	MF, PP	190	11	39	R,H	H	H	H	R,H
	W2	MF, PP	250	13	47	R,H	H	H	H	R,H
	W3	FY, PP	284	20	48	R,H	R,H	R,H	R,H	R,H
	W4	MU, PET	290	16	70	R,H	R,H	R,H	R,H	R,H
	W5	FY, PP	490	35	70	R,H	R,H	R,H	R,H	R,H
	W6	FY, PP	578	44	105	R,H	R,H	R,H	R,H	R,H
	W7	MU, PET	1,907	316	632	R,H	NT	NT	NT	R,H
Geogrids	GG1	MU, PET	305	25	63	R,H	NA	NA	NA	NA
	GG2	MU, PET	387	37	102	R,H	NA	NA	NA	NA
	GG3	MU, PET	617	65	137	R,H	NA	NA	NA	NA
	GG4	MU, PET	1,284	146	371	R,H	NA	NA	NA	NA

[a]NW=nonwoven geotextile, W=woven geotextile, and GG=geogrid.

[b]NP=needle-punched; PP=polypropylene, PET=polyester, MF=monofilament, MU=multifilament, and FY=fibrillated yarn.

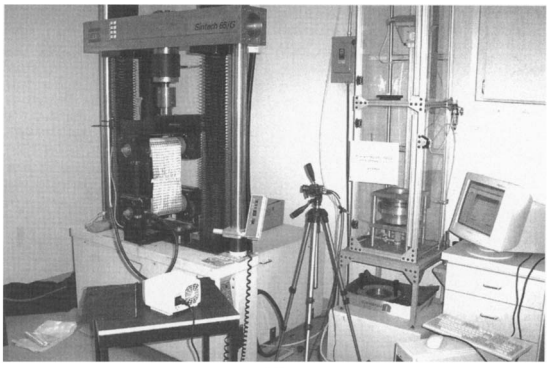
[c]R=tested with roller grips, H=tested with hydraulic grips, NA=not applicable, and NT=test was not performed.

1,828 mm in length and 250 mm in width. These widths corresponded to a geogrid longitudinal member number of 7–8. The specimen gage length was selected as 381 mm in all tests.

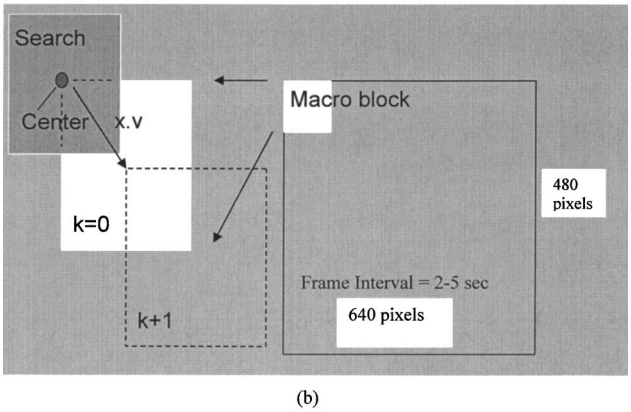
Before testing, the self-weight of the lower grip was used to remove any initial slack in the specimens. A charge-coupled device monochrome camera was mounted apart from the test setup and simultaneously captured digital pictures of the test specimens at 2 or 5 s intervals depending on the rate of displacement applied during testing [Fig. 1(a)]. Gridlines were drawn on specimen surfaces using paint markers at a 10 mm spacing to achieve the contrast that is necessary for analyses of the digital frames captured. The camera was connected to an image acquisition board providing 8-bit images at a resolution of 640×480 pixels, and controlled by a graphical user interface in *LabVIEW* installed on a Pentium microprocessor computer. The geosynthetic specimens were illuminated by fiber optic light guides to achieve uniform intensity distributions on the specimen surfaces. The image frames were saved onto the computer for subsequent strain analysis. Details of the image capturing methodology can be found in Aydilek et al. (2004).

Image Analysis Methodology

The image frames were analyzed using two different block-based matching algorithms. Block-based matching algorithms are widely used in the estimation of optical flow and pattern recognition problems due to their moderate hardware requirements and ease of implementation. The main assumption of the block-based methods is that the image frames consist of moving small rectangular blocks (called macroblocks) where flow is assumed to be constant within the block.



(a)



(b)

Fig. 1. (a) Photograph of image acquisition setup, and (b) schematic showing image analysis process

The first algorithm called BMAD was originally adopted from MPEG by rewriting it in C++ programming language and then transferring it into *LabVIEW* to create a user friendly application (Guler et al. 1999). Fundamentally, BMAD searches for a constant size of block between successive image frames based on a matching criterion [Fig. 1(b)]. Similar patterns are tracked sequentially from one image to the next and the amount of movement is calculated for each block based on Eqs. (1) and (2) to produce the optical flow map for the entire image. Guidelines on the selection of search window size and macroblock are described in detail by Guler et al. (1999).

The BMAD uses the minimum absolute difference criterion (MAD), which is given in the following form:

$$\mathrm{MAD}(d_x,d_y) = \sum |E_t(x,y) - E_{t+1}(x+d_x, y+d_y)| \tag{1}$$

$$(\hat{d}_x,\hat{d}_y)_{\min} = \arg \text{ minimum } \mathrm{MAD}(d_x,d_y) \tag{2}$$

where $(\hat{d}_x,\hat{d}_y)_{\min}$ = displacement vector corresponding to the minimum of the sum of the absolute differences between the base macroblock and scan macroblock; $E_t(x,y)$ = gray scale pixel intensity at location (x,y) at time t; and $E_{t+1}(x+d_x,y+d_y)$ = gray scale pixel intensity at location $(x+d_x,y+d_y)$ at time $t+1$.

The second block-based algorithm, NCC, was based on a commonly used technique called cross correlation. The cross-correlation technique has been widely used to analyze various phenomena in geomechanics and fluid mechanics, such as shear band formation in granular soils (Raschke et al. 1996), evaluation of sediment movements (Papanicolaou et al. 1999), and measurement of displacements in asphalt mix and soil structures (Masad et al. 2001; Liu and Iskander 2004). The cross-correlation coefficient is the cumulative product of pixel intensities between the base macroblock and the scan block and is defined by

$$\mathrm{CCR} = \sum_{x,y} E_t(x,y)E_{t+1}(x+d_x,y+d_y) \tag{3}$$

The best match is obtained when this cumulative product is maximized as defined below

$$(\hat{d}_x,\hat{d}_y)_{\max} = \arg \text{ maximum } \mathrm{CCR}(d_x,d_y) \tag{4}$$

where $(\hat{d}_x,\hat{d}_y)_{\max}$ = displacement vector that corresponds to the maximum cross correlation between the base macroblock and scan macroblock. The correlation function given in Eq. (3) has the disadvantage of being sensitive to changes in the pixel intensities $E_t(x,y)$ and $E_{t+1}(x+d_x,y+d_y)$ (Gonzales and Woods 1992; Sadek et al. 2003). Thus, the correlation function in Eq. (3) is normalized using the intensity values of matching images, as suggested by Lewis (1995) and Giachetti (2000)

$$\mathrm{NCC}(d_x,d_y) = \frac{\sum_{x,y} E_t(x,y)E_{t+1}(x+d_x,y+d_y)}{\sqrt{\sum_{x,y} E_t(x,y)^2 \sum_{x,y} E_{t+1}(x+d_x,y+d_y)^2}} \tag{5}$$

where $\mathrm{NCC}(d_x,d_y)$ = normalized cross-correlation function.

The selection of the macroblock sizes is an important step in the analysis for defining the correct match of features between two consecutive frames. Based on a recent study conducted by

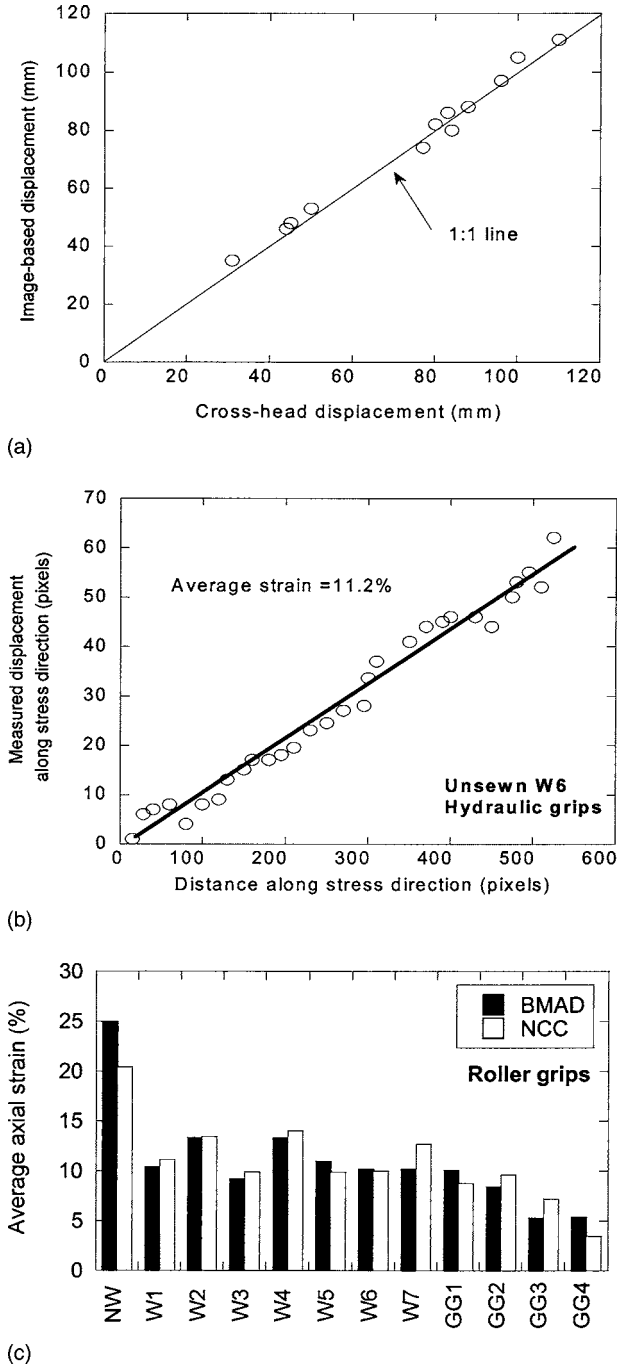


Fig. 2. (a) Comparison of image-based and cross-head displacements for geosynthetics tested in hydraulic grips; (b) displacement versus distance graph for unsewn woven geotextile W6 tested in hydraulic grips; and (c) comparison of axial strains determined by block-based minimum absolute difference and normalized cross correlation for geosynthetics tested in roller grips

Aydilek et al. (2004), a macroblock size of 16×12 pixels was chosen and used throughout the analysis. In order to check the accuracy of optical flow-based methodologies, the cross-head displacements of twelve different geosynthetics registered by the laboratory tension test machine were compared to the displacements calculated by one of the image-based algorithms, BMAD. Fig. 2(a) presents this comparison for the specimens tested using the hydraulic grips. An excellent agreement can be observed between the cross-head displacements recorded by the tension machine and the image-based displacements, which confirms the validity of the image-based approach. Detailed verification of the image-based approach to define geosynthetic strain distributions can be found in Aydilek et al. (2004).

Average Axial Strain

In order to analyze the strains for each geosynthetic specimen, measured displacements were plotted against the length of the image. The slope of the best fitted line to the data provides the average axial strain. Fig. 2(b) shows the measured displacement values and calculated average axial strain at failure for one of the woven geotextiles, W6. A preliminary analysis indicated that the type of optical flow technique (i.e., BMAD versus NCC) did not significantly affect the average axial strain measurements. Fig. 2(c) shows this effect for all the geosynthetics tested. The difference between the two strains is small, ranging from 0.1 to 4.5%. Therefore, BMAD was chosen and used throughout the analysis.

Results

Effect of Geosynthetic and Clamping Type on Strain Distributions

Figs. 3 and 4 show the lateral versus axial strains in the geosynthetics tested with the hydraulic and roller grips, respectively. During the analyses of images, the lateral strains were calculated at every location within each specimen and the maximum of these lateral strains was chosen and reported herein. Therefore, the term "lateral strain" used in the following sections will be referred to as the maximum lateral strain (contraction) that occurred in the specimen at any given axial strain. The results indicate that the lateral strains were small at a 3% axial strain, which is a limit reported by Allen and Bathurst (2002) to generate failure zones in reinforced structures. The lateral strains at this limit range from 0.3 to 1.9%. A strain value as high as 4.9% was measured for one of the PET woven geotextiles (W4). As expected, the nonwoven geotextile exhibits the highest axial and lateral strain values at failure conditions. The lateral strain measured for this geotextile at failure is about 67%, which is significantly higher than the strains measured for other geosynthetics. The lateral strain is negligible up to about 3% of the axial strain of the PP woven geotextiles and geogrids. The contraction is evident after this point and continues until the specimens reach their failure points. The lateral strains at failure for the woven geotextiles and geogrids stay in a narrow range between 2 and 8%, comparable with the findings of Shinoda and Bathurst (2004a). The only exception to that is the two PET woven geotextiles (W4 and W7), for which relatively higher lateral strains were recorded due to the high-stretch capacity of their polyester yarns. The lateral strain values at failure range from 12 to 25% for these two geotextiles.

As seen in Figs. 3 and 4, the lateral strain is lower than the axial strain for the geogrids and PP wovens, when the failure condition is considered. Conversely, the lateral strain is generally higher than the axial strain for NW and the two PET woven geotextiles (W4 and W7). For instance, the ratio of lateral strain-to-axial strain at failure (i.e., $\varepsilon_L/\varepsilon_A$) is approximately 2.1 and 1.6 for NW and W4, respectively, whereas the same ratio ranges from 0.26 to 0.66 for the geogrids when tested with roller grips.

The geosynthetics employed in the current study were tested using two types of grips to evaluate the clamping effects on strain

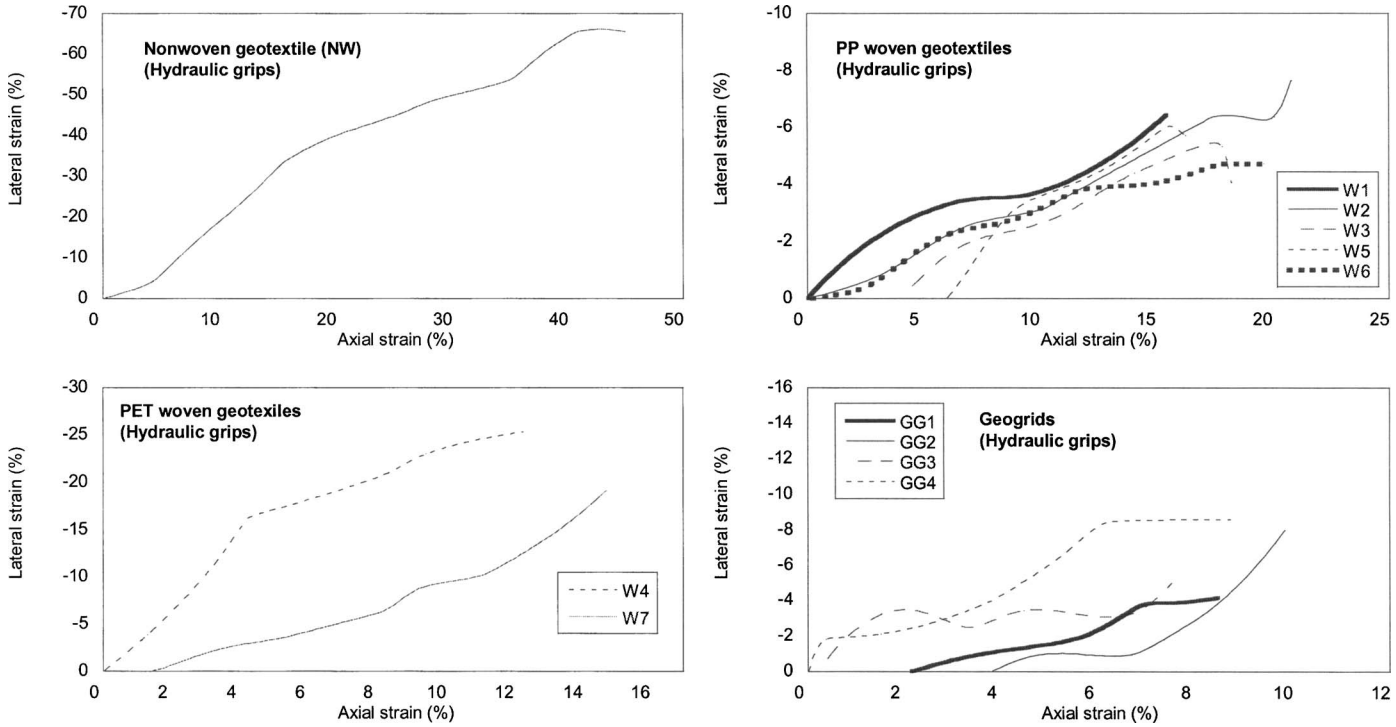


Fig. 3. Strain distributions in unsewn geosynthetics tested in hydraulic grips

distributions. Hydraulic grips have traditionally been used in wide-width tensile testing of nonwoven geotextiles and low strength woven geotextiles. However, for geotextiles with ultimate strengths above 50–90 kN/m, the standard hydraulic grips may not be satisfactory due to slippage in the grips or stress concentrations around the grip locations (Koerner 1999). When testing such geotextiles and geogrids, roller grips are recommended because the geosynthetic tightens on itself around the rollers and the failure occurs within the specimen between the two rollers (Skochdopole et al. 2000). In spite of those recommendations, the use of hydraulic grips for testing high-strength geosynthetics is not uncommon (Kelkar et al. 2000; Müller-

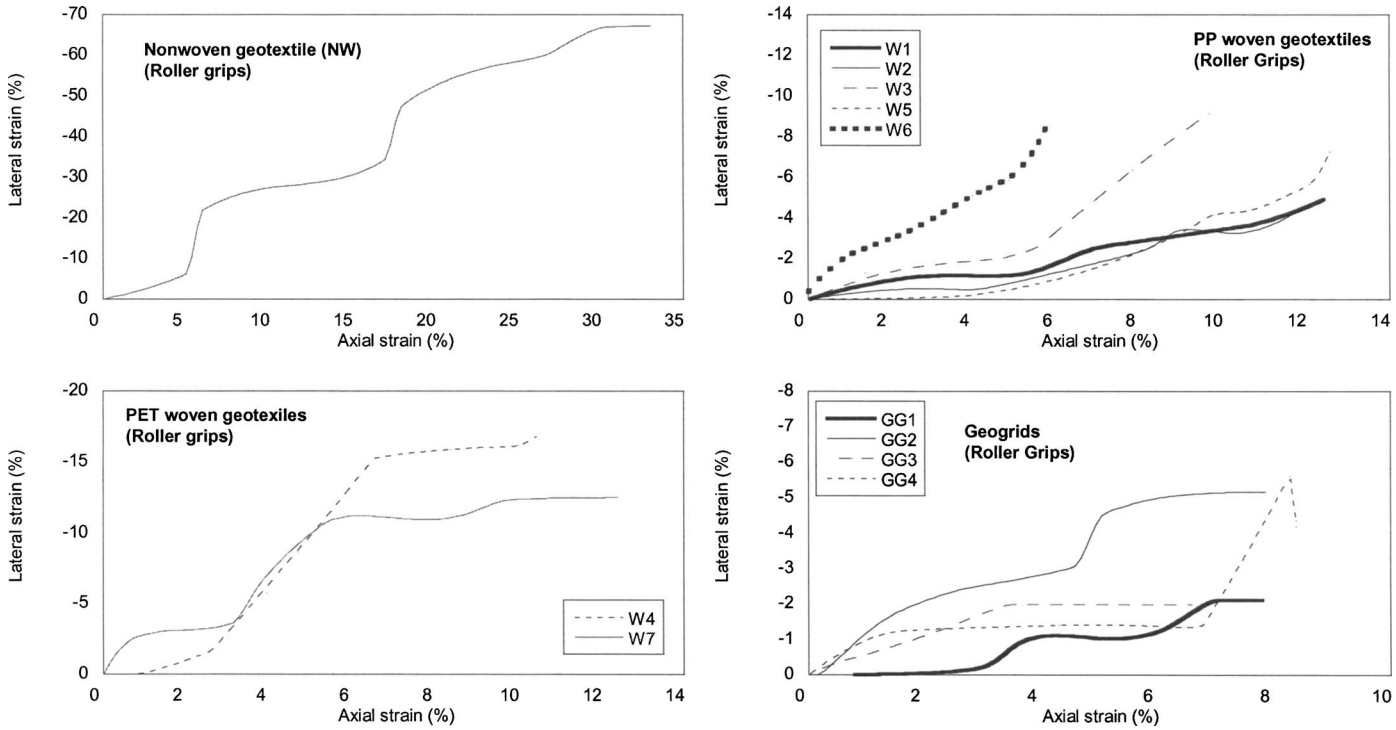


Fig. 4. Strain distributions in unsewn geosynthetics tested in roller grips

Table 2. Lateral Strain-to-Axial Strain Ratios ($\varepsilon_L/\varepsilon_A$) at Failure for Geosynthetics Tested in Two Different Grips

			Hydraulic grips				Roller grips			
Type	Geosynthetic ID[a]	Structure[b]	Unsewn	Butterfly seam	Flat seam	J seam	Unsewn	Butterfly seam	Flat seam	J seam
Nonwoven Geotextile	NW	NP, PP	1.73	0.68	0.77	0.78	2.1	NT[d]	NT[d]	NT[d]
Woven Geotextiles	W1	MF, PP	0.41	0.38	0.35	0.33	0.4	NT[d]	NT[d]	NT[d]
	W2	MF, PP	0.39	0.21	0.38	0.29	0.39	NT[d]	NT[d]	NT[d]
	W3	FY, PP	0.23	0.21	0.19	0.22	0.94	0.39	0.65	0.4
	W4	MU, PET	2.05	0.36	0.41	0.39	1.6	0.76	0.5	0.77
	W5	FY, PP	0.35	0.3	0.33	0.29	0.58	0.27	0.46	0.77
	W6	FY, PP	0.25	0.21	0.24	0.16	1.46	0.35	0.16	0.2
	W7	MU, PET	1.35	NT[d]	NT[d]	NT[d]	1.0	NT[d]	NT[d]	NT[d]
Geogrids	GG1	MU, PET	0.55	NA[c]	NA[c]	NA[c]	0.26	NA[c]	NA[c]	NA[c]
	GG2	MU, PET	0.81	NA[c]	NA[c]	NA[c]	0.66	NA[c]	NA[c]	NA[c]
	GG3	MU, PET	0.67	NA[c]	NA[c]	NA[c]	0.3	NA[c]	NA[c]	NA[c]
	GG4	MU, PET	0.98	NA[c]	NA[c]	NA[c]	0.52	NA[c]	NA[c]	NA[c]

[a]NW=nonwoven geotextile; W=woven geotextile; and GG=geogrid.

[b]NP=needle-punched; PP=polypropylene; PET=polyester; MF=monofilament; MU=multifilament; and FY=fibrillated yarn.

[c]NA=not applicable.

[d]NT=test was not performed.

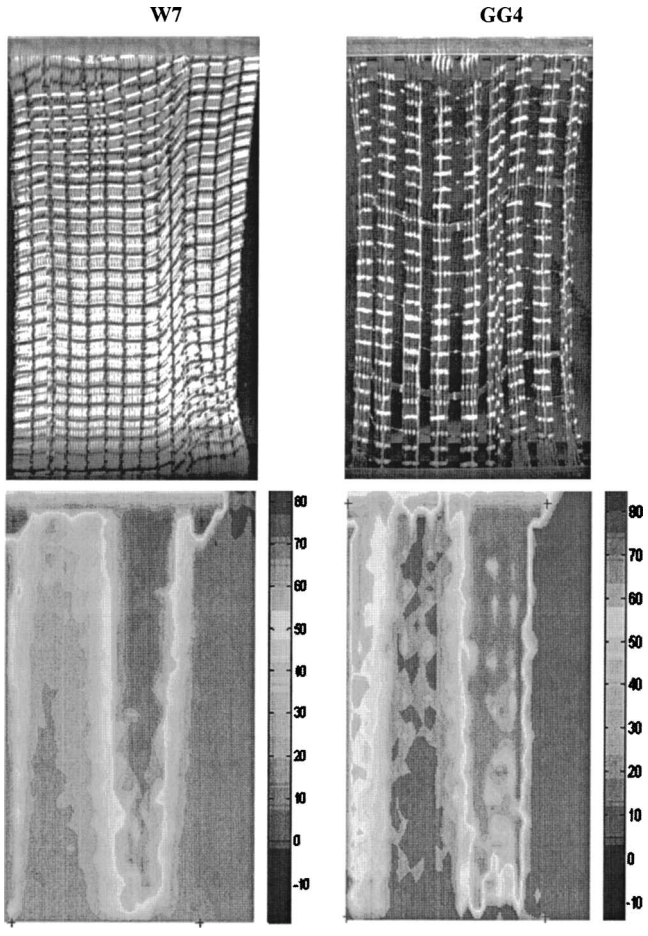


Fig. 5. Images and displacement contours of two geosynthetics experienced slippage at failure during tensile testing in hydraulic grips (displacements are given in units of pixel)

Rochholz and Recker 2000). The results presented in Figs. 3 and 4 indicate that the use of roller grips generally results in relatively lower axial strains at failure for the geotextiles.

The $\varepsilon_L/\varepsilon_A$ ratios summarized in Table 2 show that the ratio does not change for the monofilament PP wovens (W1 and W2), and decreases significantly for the NW and fibrillated-yarn PP wovens when the specimens are tested in the hydraulic grips rather than the roller grips. On the other hand, the $\varepsilon_L/\varepsilon_A$ ratio increases for geogrids and the PET wovens when the hydraulic grips are preferred for testing. For instance, the $\varepsilon_L/\varepsilon_A$ ratio for W7 increases from 1.0 to 1.35 when the hydraulic grips are used rather than the roller grips. This woven geotextile has a very high ultimate strength value ($\sigma_{ultimate}$=632 kN/m), and wide-width tensile tests have traditionally been conducted using roller grips. Visual observations during the testing of W7 with the hydraulic grips showed that slippage occurred around the moving (upper) grip area. It is believed that the tensile loads transferred to the

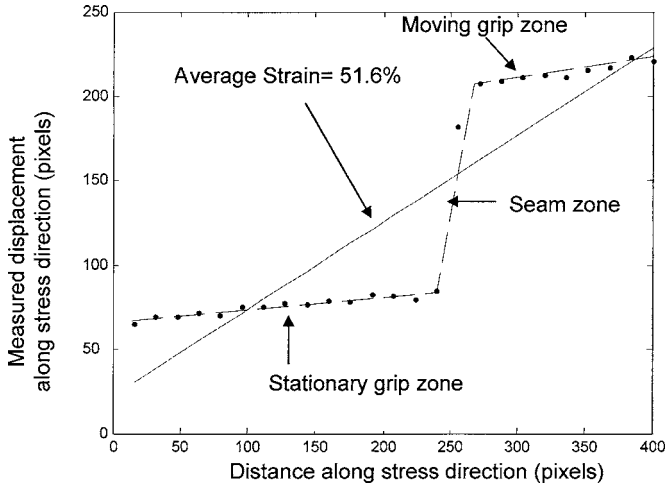


Fig. 6. Displacement versus distance relationship for geotextile W3 sewn with butterfly type seam and tested in roller grips

specimen were not uniform and were applied to a smaller section of the specimen width due to the slippage. This phenomenon, in turn, dramatically increased stresses within some fibers and eventually initiated an early failure without developing further axial strains. As a result, the ratio of $\varepsilon_L/\varepsilon_A$ increased for the tested specimen. The digital image of W7 at the verge of failure and its corresponding displacement contours are given in Fig. 5 to demonstrate this phenomenon. It is clear from the figure that the left-hand side of the geotextile did not fully stretch due to slippage, whereas the right-hand side experienced a significant amount of displacement (note the relatively darker grayish zones in the geotextile). Furthermore, localized displacements occurred within the upper grip area.

The geogrids exhibit relatively higher lateral strains when tested with the hydraulic grips, as presented in Figs. 3 and 4. The $\varepsilon_L/\varepsilon_A$ ratio increases from 0.26 to 0.66 to a range of 0.55–0.98 when the hydraulic grips are used rather than the roller grips (Table 2). Similarly, Shinoda and Bathurst (2004a) reported low $\varepsilon_L/\varepsilon_A$ ratios (~0.07) for PET geogrids when tested using roller grips. The ratios determined in the current study are higher than those measured by Shinoda and Bathurst (2004a), and the difference may be attributed to the use of geogrids that have significantly higher strengths. The relatively higher $\varepsilon_L/\varepsilon_A$ ratios obtained with hydraulic grips are as a result of the specimen slippage within the grips. The digital image of the specimen GG4 at failure and its corresponding displacement contours given in Fig. 5 are evidence of this slippage. The slipped area in the center experiences very little displacement as compared to other parts of the geogrid specimen, including the upper grip area.

Effect of Seam Presence on Strain Distributions

The BMAD algorithm was used to evaluate the strain distributions in geotextiles sewn with three commonly used seam types: butterfly, flat, and J-seam. Preliminary observations showed that three distinct zones were evident when measured displacements were plotted against the cross machine direction of the captured images, as illustrated in Fig. 6 for W3. It can be observed from Fig. 6 that the use of an average axial strain value for the entire specimen would be misleading and the strains should be calculated separately for the two grip zones (i.e., stationary and moving grip zones), as well as for the seam zone. The contour plots of strain also showed that it is necessary to calculate the average axial strains separately for each region. One set of these plots developed for W1 tested in the hydraulic grips is given in Fig. 7, as an example to demonstrate this phenomenon. As seen in Fig. 7, the seam area results in significantly higher axial strains as compared to the two zones located above and below the seam (i.e., two grip zones). These results indicated that the image-based procedure, BMAD, has a significant advantage since three distinct slopes that are observed at any time during testing of the specimens can be used to define the progressive failure of the seams, even though such a time-dependent analysis was not conducted in the current study.

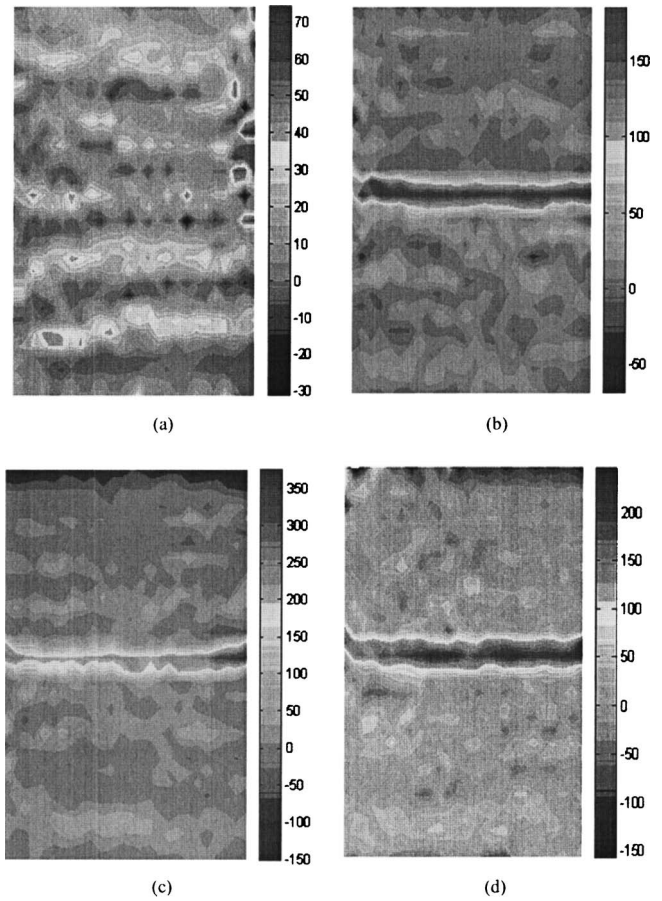


Fig. 7. Distributions of axial strain at failure for W1 tested in hydraulic grips: (a) no seam, (b) butterfly, (c) flat, and (d) J seam (all strains are given as percentage values)

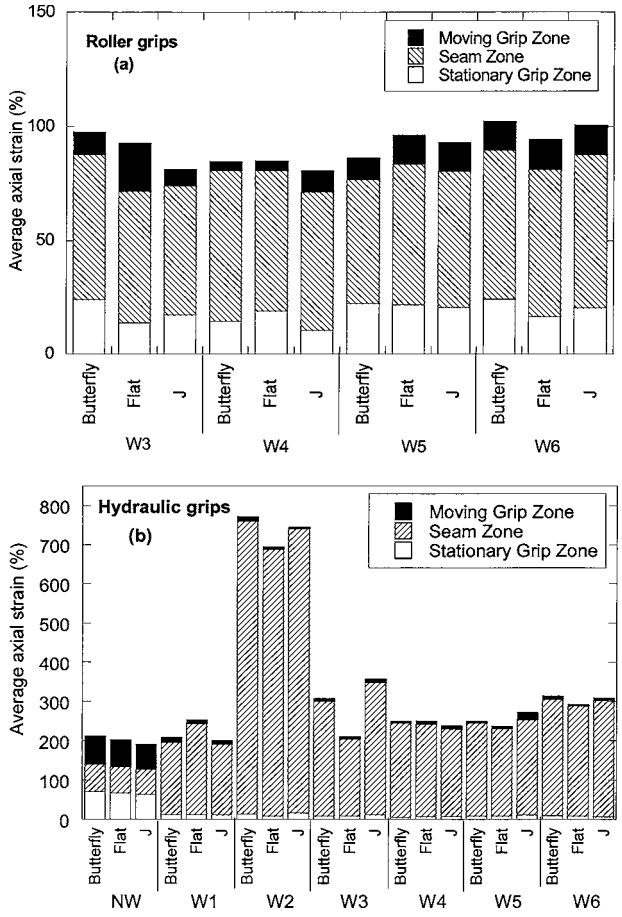


Fig. 8. Strain values at different zones within geosynthetic specimens tested in two different grips

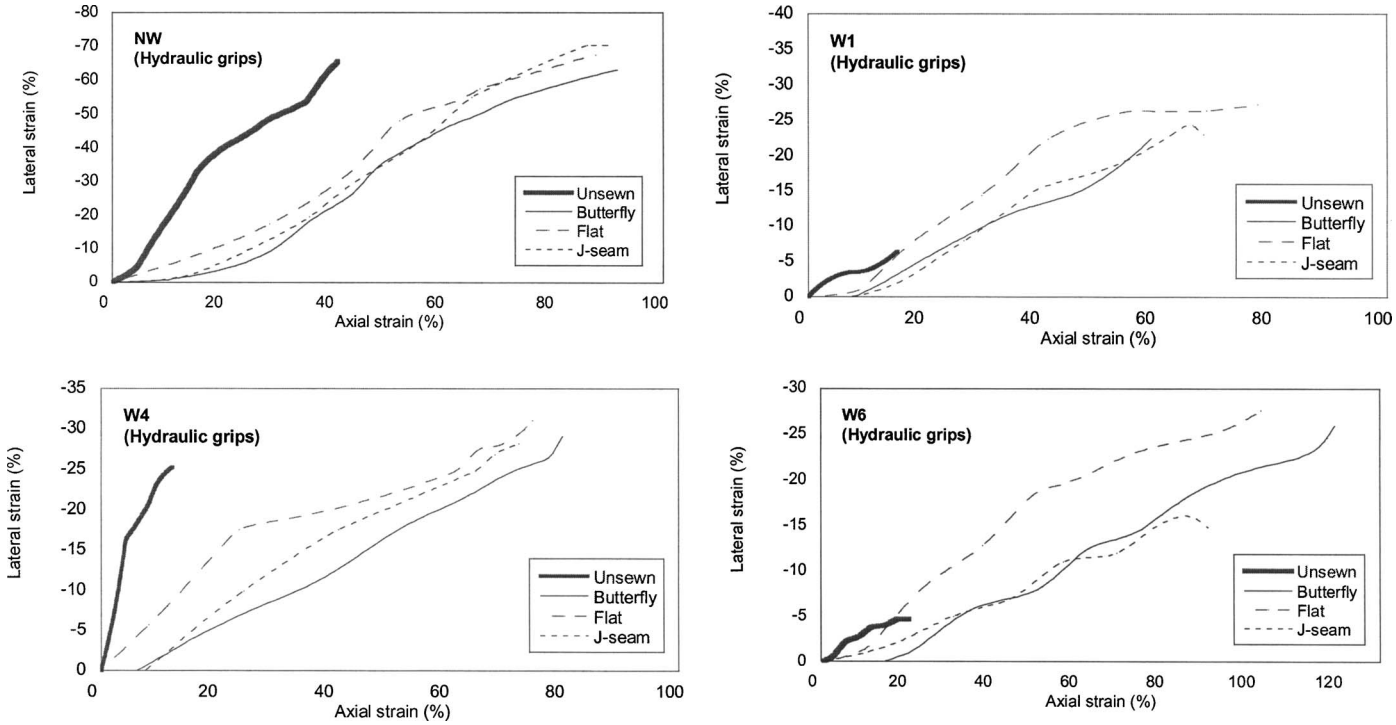


Fig. 9. Strain distributions in sewn geosynthetics tested in hydraulic grips

Fig. 8 presents the average axial strain values at failure in the two grip zones and seam locations of the geotextiles. For all specimens, a substantial amount of strain developed in the vicinity of seams regardless of the clamping technique used. This can be expected since the sewing process weakens the geotextile and causes large strain variations around the seam zone. As seen in Fig. 8(a), the average axial strain within the seam zones stays in a range of 70–75% for all of the geosynthetics, while the average axial strain is about 20% and less than 15% around the moving and stationary grip locations, respectively, when testing is performed with roller grips. When tests are conducted with the hydraulic grips, on the other hand, the strain distribution is dependent on the type of geosynthetic [Fig. 8(b)]. Larger variations in the average axial strain can be observed for woven geotextiles,

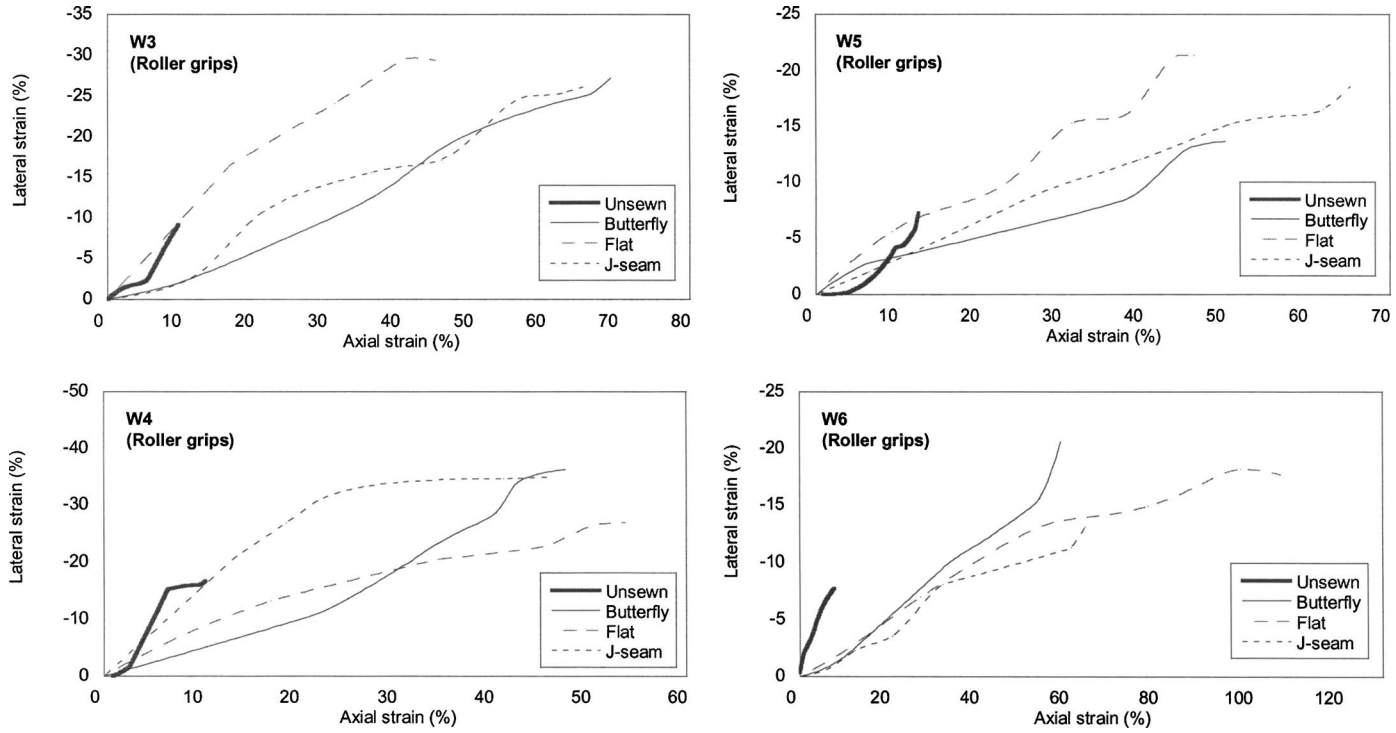


Fig. 10. Strain distributions in sewn geosynthetics tested in roller grips

whereas these strains are comparable at different zones inside the nonwoven geotextile. It is interesting to note that the strain magnitude reached for geotextiles is higher when they are tested using the hydraulic grips rather than the roller grips (e.g., up to 300% versus up to 100% for geotextile W6).

As seen in Figs. 9 and 10, sewing a geotextile increases its axial strain at failure (ε_A), regardless of the clamping technique used. For instance, ε_A increases about 2.4 times for the nonwoven geotextile, whereas the increase is in a range of 3.8–6.5 times for the woven geotextiles when the hydraulic grips are used. Additionally, ε_A increases 3.6–18 times due to sewing when the geotextiles are tested in roller grips. Similar observations were made for W2, W3, and W5 tested in the hydraulic grips, even though their lateral strain versus axial strain plots are not presented herein for brevity. Table 2 shows that the lateral strain-to-axial strain ratio ($\varepsilon_L/\varepsilon_A$) is generally lower for the sewn geotextiles when either hydraulic or roller grips are used; however, a conclusion cannot be reached whether a particular seaming type necessarily causes a greater contraction or not. The lower $\varepsilon_L/\varepsilon_A$ ratios observed due to seaming are probably due to the stiff zone introduced by the threads during the seaming process, which resists the contraction.

Effect of Puncturing on Strain Distributions

Geotextiles are occasionally vulnerable to puncture during field installation and the punctured region may have an effect on the strain distribution of the fabric. These punctured zones may not affect the overall performance of retaining walls or bridge abutments; however, they may cause unexpected failures during capping of soft sediments and sludges especially if the hole diameter is large. As part of the current study, 8 mm diameter holes were opened on samples of virgin geotextiles according to *ASTM D 4833* (ASTM 2001a) to simulate puncturing occurring in the field. Fig. 11 summarizes the effect of puncture on the strain distributions within unsewn and sewn specimens. The average axial strain appears to be insensitive to puncture regardless of either the geotextile type or the clamping technique, except for the NW. The small variations in average axial strains are attributed to the material properties within the same roll. The lateral versus axial strain plots for virgin and punctured specimens of a particular geotextile were highly comparable, even though the results are not presented herein. The images captured during testing showed that the failure indicated by the tear spreads outward from the initial puncture in the geotextile. Fig. 12 is given as an example to demonstrate this phenomenon for W1. The tests performed on the specimens suggested that localized strains occur in the vicinity of the puncture zone, despite the fact that the diameter of the hole opened in the center of the geotextiles in this study was small. The maximum axial strain occurred in the vicinity of the punctured zone was about 100–150 times higher than the strain elsewhere in the specimen. It is believed that a detailed study is necessary to investigate the effect of hole diameter on the overall strain distribution.

Conclusions

Determining the deformation response of geosynthetics under load is important in developing an in-depth understanding of the engineering behavior of these materials. The accurate determination of localized strains and their respective zones becomes particularly critical for design purposes in the presence of seams, punctured zones, or possible defects that occurred during production since the presence of such nonuniformities affect the overall strain distribution. Twelve different geosynthetics along with their sewn and punctured companions were subjected to wide-width tensile tests using roller and hydraulic grips in the current study. Digital images of specimens were captured during testing, and analyses of time-lapsed images were performed using two optical flow techniques to define the strain distributions within the specimen as well as in the vicinity of the grip locations and seams.

The following conclusions are advanced:

1. The image-based optical flow technique used in this study defines the distribution of strains in a geosynthetic during tensile testing. The technique can measure the localized strains in the vicinity of test grips, seams, and punctured zones. An excellent agreement was observed with the measured (i.e., the machine's cross-head) and image-based displacements.
2. The results indicated that the lateral strains are small and range from 0.3 to 4.9% at 3% axial strain, a limit reported by previous researchers to generate failure zones in the reinforced structures. The largest strain value at this limit was measured for one of the polyester (PET) woven geotextiles. The nonwoven geotextile exhibited the highest axial and lateral strain values at failure. The lateral strain was negligible up to about 3% of the axial strain of the polypropylene (PP) woven geotextiles and geogrids, and the lateral strains at failure stayed in a range of 2–8% for these geosynthetics. On the other hand, the PET woven geotextiles experienced large lateral strain values at failure.
3. The lateral strain was greater than the axial strain at failure for the nonwoven geotextile and PET wovens, and the ratio of lateral strain-to-axial strain at failure ($\varepsilon_L/\varepsilon_A$) ranged from 1.0 to 2.1. On the other hand, the same ratio stayed in a range of 0.3–0.81 for geogrids depending on the clamping technique used. The data suggest that caution should be exercised when nonwoven or PET wovens are used in critical applications that are likely to experience high axial and lateral strains, such as hydraulic filling of geotextile containers and capping of high water content geomaterials.
4. Slippage of the high-strength PET wovens and geogrids were observed during testing those geosynthetics in hydraulic grips. The $\varepsilon_L/\varepsilon_A$ ratio increased for the geogrids and the PET wovens when hydraulic grips were used. This increase occurred as a result of slippage at the upper grip location, in-

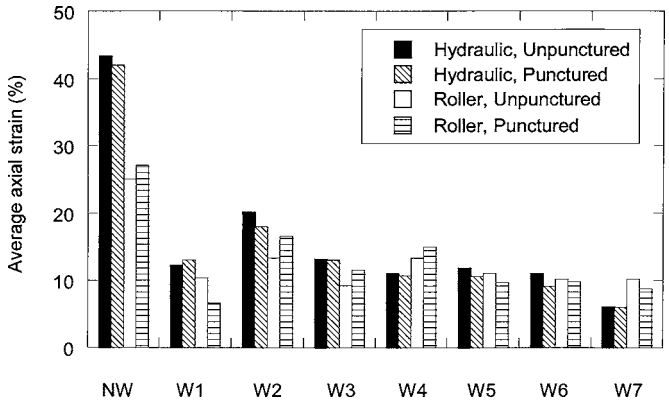


Fig. 11. Average axial strains for punctured and unpunctured specimens tested in two different grips

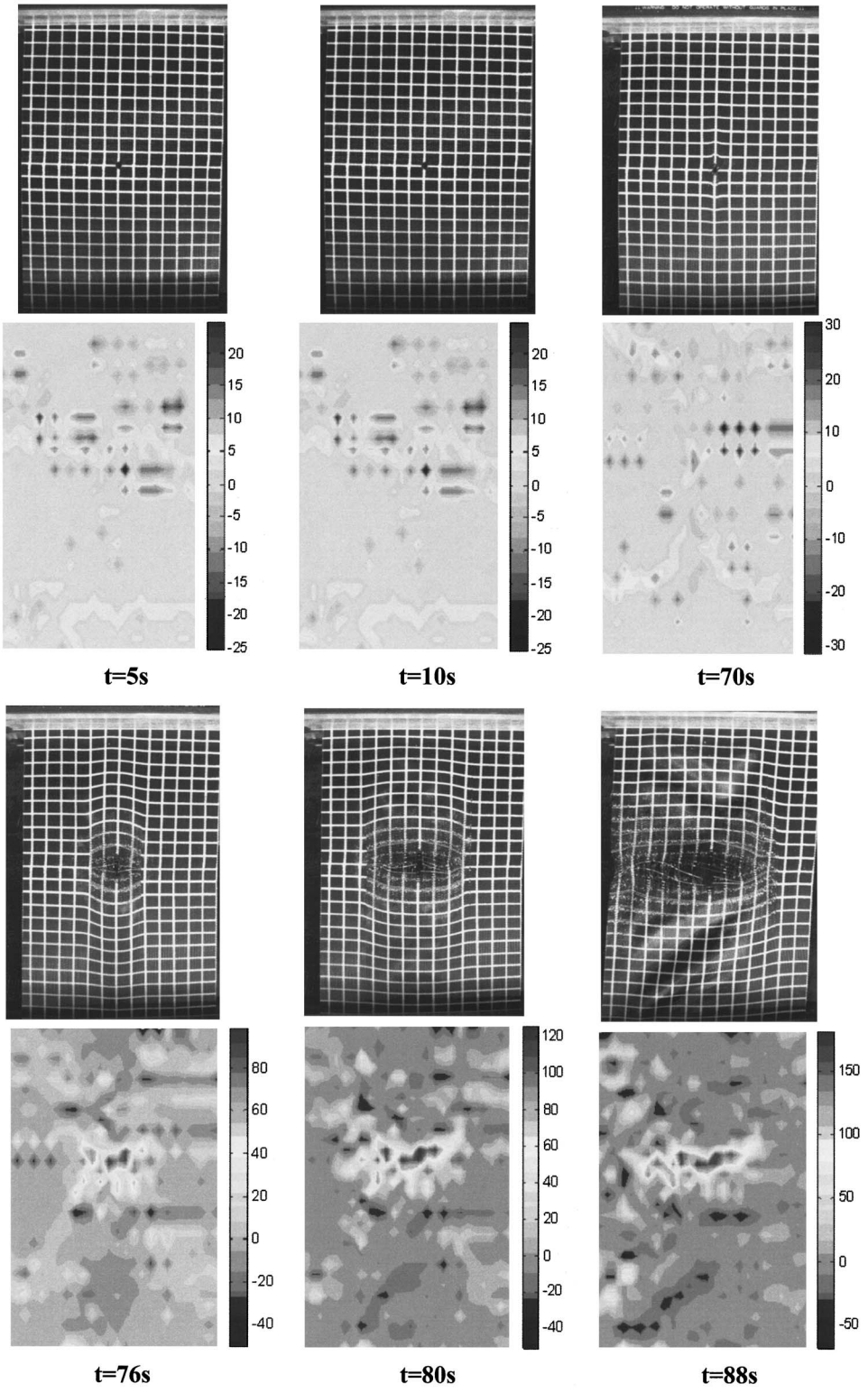


Fig. 12. Development of failure around puncture in W1 tested in hydraulic grips (all axial strains are given as percentage values)

dicating that use of hydraulic grips should be avoided in their testing.

5. For all of the specimens, a substantial amount of strain developed in the vicinity of seams regardless of the clamping technique used. The strains in the vicinity of seams were significantly higher, when testing was conducted with hydraulic grips rather than roller grips (up to 75% versus 747%). Sewn geotextiles experienced higher axial strains and lower $\varepsilon_L/\varepsilon_A$ ratios at failure.
6. The average axial strain appears to be insensitive to puncture regardless of the clamping method. The tests performed on the specimens suggested that localized strains that occur in the vicinity of the puncture zone. The maximum axial strain that occurred around the punctured zone was about 100–150

times higher than the strain elsewhere in the specimen.

7. The existing load-strain-time models for geosynthetic reinforcement products are typically one dimensional. The data presented in this paper demonstrated that a two-dimensional response should be considered in development of future constitutive models (Shinoda and Bathurst 2004a), in particular for some of the geosynthetic products (e.g., PET woven geotextiles) or for applications in which large strains are likely to be experienced (e.g., geotextile containers).

Acknowledgments

The funding for this project was provided by the University of Maryland through General Research Board Award given to the third writer. Additional funding was provided by the Minta Martin Fund through the Department of Aerospace Engineering while the second writer was a post-doctoral research associate at the University of Maryland. All this support is gratefully acknowledged.

References

Allen, T. M., and Bathurst, R. J. (2002). "Soil reinforcement loads in geosynthetics walls at working stresses." *Geosynthet. Int.*, 9(5–6), 525–566.

(ASTM). (2001a). "Standard test method for index puncture resistance of geotextiles, geomembranes, and related products." *ASTM D 4833*, West Conshohocken, Pa.

American Society for Testing and Materials (ASTM). (2001b). "Standard test method for tensile properties of geotextiles by the wide-width strip method." *ASTM D 4595*, West Conshohocken, Pa.

Aydilek, A. H., Guler, M., and Edil, T. B. (2004). "Use of image analysis in determination of strain distribution during geosynthetic tensile testing." *J. Comput. Civ. Eng.*, 18(1), 65–74.

Bais-Singh, S., and Goswami, B. C. (1996). "Deformation behavior of spun-bonded nonwovens: Measurement." *Proc., INDA-TEC 96*, Crystal City, Va., 29.1–29.19.

Billard, J. W., and Wu, J. T. H. (1991). "Load test of a large scale geotextile-reinforced retaining walls." *Proc., Geosynthetics '91*, IFAI, Vol. 2, St. Paul, Minn., 537–548.

Chew, S. H., Wong, W. K., Ng, C. C., Tan, S. A., and Karunaratne, G. P. (2000). "Strain gauging geotextiles using external gauge attachment method." *Grips, clamps, clamping techniques and strain measurement for testing of geosynthetics, ASTM STP 1379*, P. E. Stevenson, ed., American Society for Testing and Materials, West Conshohocken, Pa.

Edil, T. B., and Aydilek, A. H. (2001). "Geotechnics of capping very soft wastes." *Proc., 13th Int. Conf. on Soil Mechanics and Geotechnical Engineering*, Vol. 3, Istanbul, Turkey, 1903–1906.

Giachetti, A. (2000). "Matching techniques to compute image motion." *Image Vis. Comput.*, 18, 247–260.

Gonzales, R. C., and Woods, R. E. (1992). "Digital image processing." Addison Wesley, Boston.

Guler, M., Edil, T. B., and Bosscher, P. J. (1999). "Measurement of particle movement in granular soils using image analysis." *J. Comput. Civ. Eng.*, 13(2), 116–122.

Kelkar, A. D., Stevenson, P. E., Skochdopole, T. R., and Yarmolenko, S. N. (2000). "Effect of gage length and test speed on the measured tensile properties of geosynthetic reinforcements." *Grips, Clamps, Clamping Techniques, and Strain Measurement for Testing of Geosynthetics, ASTM STP 1379*, P. E. Stevenson, ed., West Conshohocken, Pa., 37–46.

Koerner, R. M. (1999). *Designing with geosynthetics*, 4th Ed., Prentice–Hall, Englewood Cliffs, N.J.

Lewis, J. P. (1995). "Fast template matching." *Proc., Vision Interface 95*, Quebec City, Quebec, 120–123.

Liu, J., and Iskander, M. (2004). "Adaptive cross correlation for imaging displacements in soils." *J. Comput. Civ. Eng.*, 18(1), 46–57.

Masad, E., Somadevan, N., Bahia, H., and Kose, S. (2001). "Modeling and experimental measurements of strain distribution in asphalt mixes." *J. Transp. Eng.*, 127(6), 477–485.

Müller-Rochholz, J., and Recker, C. (2000). "Tensile strength and clamping of geogrids." *Grips, clamps, clamping techniques, and strain measurement for testing of geosynthetics, ASTM STP 1379*, P. E. Stevenson, ed., Philadelphia, 28–36.

Papanicolaou, A. N., Diplas, P., Balakrishnan, M., and Dancey, C. L. (1999). "Computer vision technique for tracking bed load movement." *J. Comput. Civ. Eng.*, 13(2), 71–79.

Raschke, S. A., Hryciw, R. D., and Donohoe, G. W. (1996). "Microdeformations in sands by digital image processing and analysis." *Transportation Research Record*, *1548*, Transportation Research Board, Washington, D.C., 31–37.

Raymond, G. P. (1994). "Durability of geotextiles in railroad rehabilitations." *Transportation Research Board*, *1439*, Transportation Research Record, Washington, D.C., 12–19.

Sadek, S., Iskander, M. G., and Liu, J. (2003). "Accuracy of digital image correlation for measuring deformations in transparent media." *J. Comput. Civ. Eng.*, 17(2), 88–96.

Shinoda, M., and Bathurst, R. J. (2004a). "Lateral and axial deformation of PP, HDPE, and PET geogrids under tensile load." *Geotext. Geomembr.*, 22(4), 205–222.

Shinoda, M., and Bathurst, R. J. (2004b). "Strain measurement of geogrids using a video extensometer technique." *Geotech. Test. J.*, 27(5), 456–463.

Skochdopole, T. R., Cassady, L., Pihs, D., and Stevenson, P. E. (2000). "Comparative study of roller and wedge grips for tensile testing of high strength fabrics with laser extensometry." *Grips, clamps, clamping techniques, and strain measurement for testing of geosynthetics, ASTM STP 1379*, P. E. Stevenson, ed., Philadelphia, 68–82.